



**Table S2.** Dissociation constants ( $K_d$ 's), free energies ( $\Delta G$ ) and difference in free energies ( $\Delta\Delta G$ ) determined for attenuators with gGRAAu tetraloops at 15 mM Mg(OAc)<sub>2</sub> and 10°C. The anticipated secondary structure for each molecule is also the one predicted to be the most stable by Mfold (41). We have indicated the calculated free energy change of PK pairing formation (in kcal/mol at 37°C) according to Freier and colleagues (46): between brackets, is indicated whether the PK\_forming conformer is predicted (yes) or not (no) by KineFold (42) or/and Cylofold (63).

Name	Receptor	PKL	PK pairing stability and PK prediction	Kd (nM)	$\Delta G$ (kcal/mol)	$\Delta\Delta G$ (kcal/mol)
<b>Controls</b>						$\Delta\Delta G_{HD} = \Delta G(HD\_x) - \Delta G(HD\_1)$
HD_1	11nt_AA	None	-	198±34	-8.68	-
HD_4	11nt_AC	None	-	259±50	-8.53	0.15±0.05
HD_7	11nt_GU	None	-	252±29	-8.54	0.14±0.05
HD_14	11nt_A/CC	None	-	425±23	-8.25	0.43±0.10
HD_16	R1	None	-	112±29	-9	-0.32±0.05
HD_1b	11nt_AA	helix	-	339±71	-8.38	0.3±0.12
HD_7b	11nt_GU	helix	-	379±63	-8.31	0.23±0.1
<b>3' PK attenuators</b>						$\Delta\Delta G_{AT} = \Delta G(x) - \Delta G(HD\_x)$
1	11nt_AA	3`KL_AA	-3.3 (yes)	221±19	-8.62	0.06±0.03
2	11nt_AA	3`KL_AC	-(no)	323±31	-8.44	0.24±0.1
3	11nt_AA	3`KL_GU	-(no)	240±44	-8.58	0.1±0.05
4	11nt_AC	3`KL_AC	-4.8 (yes)	1356±263	-7.53	1±0.06
5	11nt_AC	3`KL_AA	-(no)	250±22	-8.55	-0.02±0.01
6	11nt_AC	3`KL_GU	-(no)	385±33	-8.31	0.22±0.04
7	11nt_GU	3`KL_GU	-5.3 (yes)	>80000	(-5.3)<	>3.24
8	11nt_GU	3`KL_AC	-(no)	479±25	-8.18	0.36±0.01
9	11nt_GU	3`KL_AA	-(no)	359±72	-8.34	0.2±0.03
16	R1	3`KL_GU	-5.3 (yes)	5276±219	-6.83	2.17±0.1
1_a	11nt_AA	3`KL_AA-5A	-3.3 (no)	485±128	-8.18	0.5±0.03
7_a	11nt_GU	3`KL_GU-5A	-5.3 (yes)	>80000	(-5.3)<	>3.24
16_a	R1	3`KL_GU-5A	-5.3 (yes)	5321±517	-6.83	2.17±0.11
<b>5' PK attenuators</b>						$\Delta\Delta G_{AT} = \Delta G(x) - \Delta G(HD\_x)$
10	11nt_AA	5`KL	-0.6 (no)	110±18	-9.01	-0.33±0.04
11	11nt_AA	5`KL_A/CC	-(no)	134±22	-8.9	-0.22±0.01
12	11nt_GU	5`KL	-0.6 (no)	298±39	-8.45	0.09±0.01
13	11nt_GU	5`KL_A/CC	-(no)	366±43	-8.33	0.21±0.05
14	11nt_A/CC	5`KL_A/CC	-3.7 (yes)	1772±135	-7.45	0.8±0.05
15	11nt_A/CC	5`KL	-(no)	568±89	-8.09	0.16±0.03
17	R1	5`KL_R1	-3.5 (yes)	3341±379	-7.09	1.91±0.12
10_a	11nt_AA	5`KL-5A	-0.6 (no)	631±280	-8.03	0.65±0.06
12_a	11nt_GU	5`KL-5A	-0.6 (no)	642±169	-8.02	0.52±0.03
17_a	R1	5`KL_R1-5A	-3.5 (yes)	7854±646	-6.61	2.39±0.16

**Table S3.** Dissociation constants ( $K_d$ 's), free energies ( $\Delta G$ ) and difference in free energies ( $\Delta\Delta G$ ) determined for heterodimer assembly with HD forming modules comprising **gGRAAU** (**gu**) or **gGRAAc** (**gc**) tetraloops, at 15 mM Mg(OAc)<sub>2</sub> and 10°C (see in Figure 2B).

Control name	Receptor	GRAA with gu or gc closing bp	Kd (nM)	$\Delta G$ (kcal/mol)	$\Delta\Delta G_{HD}$ (kcal/mol) $\Delta G(HD\_x) - \Delta G(HD\_x'')$
HD_1	11nt_AA	gu	198±34	-8.7	-
HD_1''		gc	23±3	-9.9	1.2±0.05
HD_7	11nt_GU	gu	252±29	-8.54	-
HD_7''		gc	75±13	-9.23	0.69±0.1
HD_16	R1	gu	112±29	-9	-
HD_16''		gc	49±9	-9.47	0.47±0.09

**Table S4:** Dissociation constants ( $K_d$ 's), free energies ( $\Delta G$ ) and difference in free energies ( $\Delta\Delta G$ ) determined for attenuators with gGRAAc tetraloops at 15 mM and 2 mM  $\text{Mg}(\text{OAc})_2$  and 10°C.

Name	Receptor	PKL	Kd (nM)	$\Delta G$ (kcal/mol)	$\Delta\Delta G$ (kcal/mol)
<b>15 mM Mg2+</b>					
<i>controls</i>					$\Delta\Delta G_{\text{HD}} = \Delta G(\text{HD}_{\text{x''}}) - \Delta G(\text{HD}_{\text{1''}})$
HD_1''	11nt_AA	None	23±3	-9.9	-
HD_7''	11nt_GU	None	75±13	-9.23	0.67±0.05
HD_16''	R1	None	49±9	-9.47	0.43±0.05
<i>3' PK attenuators</i>					$\Delta\Delta G_{\text{AT}} = \Delta G(\text{x''}) - \Delta G(\text{HD}_{\text{x''}})$
1''	11nt_AA	3`KL_AA	21±3	-9.94	-0.05±0.08
7''	11nt_GU	3`KL_GU	2480±424	-7.26	1.96±0.1
16''	R1	3`KL_GU	152±23	-9.09	0.65±0.1
1_a''	11nt_AA	3`KL_AA-5A	56±13	-9.39	0.49±0.16
7_a''	11nt_GU	3`KL_GU-5A	3951±771	-7	2.03±0.03
16_a''	R1	3`KL_GU-5A	96±12	-8.91	0.38±0.22
<i>5' PK attenuators</i>					$\Delta\Delta G_{\text{AT}} = \Delta G(\text{x''}) - \Delta G(\text{HD}_{\text{x''}})$
10''	11nt_AA	5`KL_AA	12±3	-10.28	-0.38±0.14
12''	11nt_GU	5`KL_GU	99±6	-9.07	-0.16±0.03
17''	R1	5`KL_R1	95±6	-8.83	0.38±0.04
10_a''	11nt_AA	5`KL_AA-5A	49±5	-9.46	-0.44±0.06
12_a''	11nt_GU	5`KL_GU-5A	53±5	-9.42	-0.11±0.05
17_a''	R1	5`KL_R1-5A	131±	-9.06	0.41±0.04
<b>2 mM Mg2+</b>					
<i>controls</i>					$\Delta G(\text{HD}_{\text{x''}}@2\text{mM}) - \Delta G(\text{HD}_{\text{x''}}@15\text{mM})$
HD_1''	11nt_AA	None	771±89	-7.91	-1.99±0.1
HD_7''	11nt_GU	None	1240±168	-7.65	-1.58±0.04
HD_16''	R1	None	995±161	-7.77	-1.7±0.07
<i>3' PK attenuators</i>					$\Delta\Delta G_{\text{AT}} = \Delta G(\text{x''}) - \Delta G(\text{HD}_{\text{x''}})$
1''	11nt_AA	3`KL_AA	1487±198	-7.55	0.36±0.04
7''	11nt_GU	3`KL_GU	>100000	(-5.3)<	>3.2
16''	R1	3`KL_GU	6797±936	-6.84	0.93±0.04
1_a''	11nt_AA	3`KL_AA-5A	843±170	-7.86	0.05±0.01
7_a''	11nt_GU	3`KL_GU-5A	>100000	(-5.3)<	>3.2
16_a''	R1	3`KL_GU-5A	6055±870	-6.7	1.01±0.07
<i>5' PK attenuators</i>					$\Delta\Delta G_{\text{AT}} = \Delta G(\text{x''}) - \Delta G(\text{HD}_{\text{x''}})$
10''	11nt_AA	5`KL_AA	1577±107	-7.51	0.4±0.4
12''	11nt_GU	5`KL_GU	4203±830	-6.96	0.68±0.11
17''	R1	5`KL_R1	6742±824	-6.69	1.08±0.07
10_a''	11nt_AA	5`KL_AA-5A	2062±211	-7.36	0.55±0.06
12_a''	11nt_GU	5`KL_GU-5A	2430±495	-7.27	0.37±0.12
17_a''	R1	5`KL_R1-5A	5198±823	-6.76	1.02±0.09

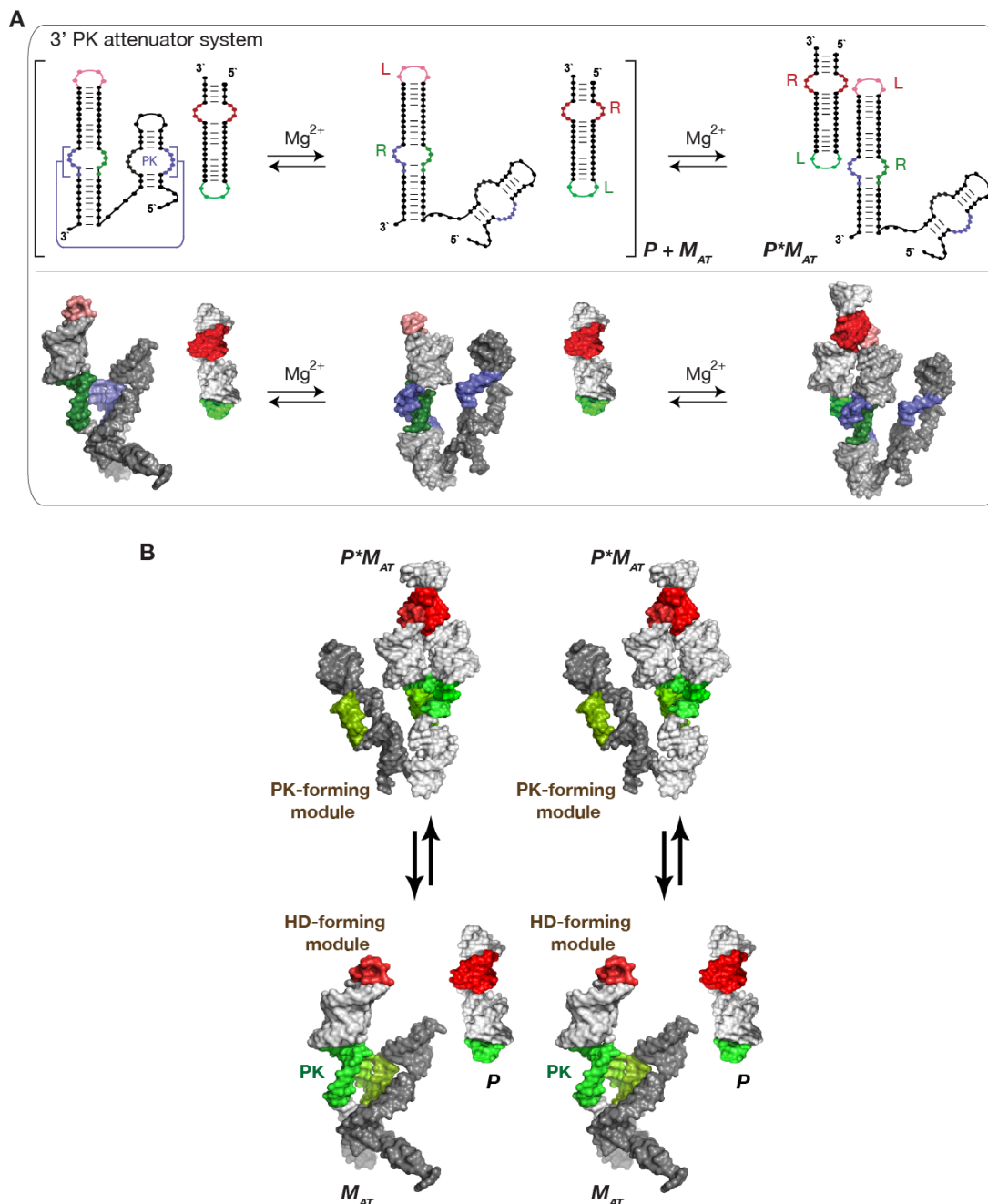
**Table S5:** Sequence analysis of GNRA/receptor interactions in class I cyclic di-GMP riboswitches based on the alignment performed by Sudarsan and colleagues (20). **A.** Distribution of GNRA/helix and GNRA/11nt (or 11nt-like) receptor interactions: the values (calculated percentages) are based on a total of 498 sequences. **B.** Analysis of the G/C content and di-nucleotide platform sequence (see also Figure S2) based on 306 class I cyclic di-GMP riboswitch sequences that contain an 11nt or 11nt-like receptor.

**A.**

Type of tetraloops	Number of GNRA loops	Number of GNRA/11nt(or 11nt-like) receptor interactions	Number of GNRA/helix receptor interactions
<b><i>GYRA Loops</i></b>	<b>177 (35.5%)</b>	<b>7 (1.4 %)</b>	<b>170 (34.1%)</b>
GUAA	36 (7%)	5 (1.0%)	31 (6.2%)
GUGA	41 (8%)	0 (0%)	41 (8.2%)
GCAA	18 (4.5%)	0 (0%)	18 (3.6%)
GCGA	82 (16%)	2 (0.4%)	80 (16.1%)
<b><i>GRRR Loops</i></b>	<b>309 (62%)</b>	<b>287 (57.6%)</b>	<b>22 (4.4%)</b>
GAAA	297 (61%)	281 (56.4%)	16 (3.2%)
GAGA	7 (2%)	5 (1.0%)	2 (0.4%)
GGAA	2 (0.4%)	1 (0.2%)	1 (0.2%)
GGGA	3 (0.6%)	0 (0%)	3 (0.6%)
<b><i>Other Loops</i></b>	<b>12 (2.5%)</b>	<b>12 (2.4%)</b>	<b>0 (0%)</b>
AAAA	2 (0.4%)	2 (0.4%)	0 (0%)
UAAA	9 (1.9%)	9 (1.8%)	0 (0%)
GGAC	1 (0.2%)	1 (0.2%)	0 (0%)
<b>TOTAL</b>	<b>498 (100%)</b>	<b>306 (61%)</b>	<b>192 (39%)</b>

**B.**

	11nt/11nt-like receptors
<b>G/C content (not including A-minor interaction)</b>	
0 G or C	12%
1 G or C	52%
2 G or C	24%
3 G or C	11%
4 G or C	1.3%
<b>Platform sequence</b>	
AA	71%
GU	8.5%
AC	7.5%
UC	5.2%
GA	2.3%
GC	0.65%
Unclassified	5.2%

**B. Supplementary Figures**

**Figure S1: Self-assembly equilibrium reactions for the 3' PK attenuator system.** (A) 3' PK attenuator system: the tectoRNA attenuator ( $M_{AT}$ ), consisting of a HD-forming module linked to a PK-forming module, can assemble with a probe (P) through their HD-forming module (reaction on the right) to form the heterodimer ( $P^*M_{AT}$ ). Attenuation of intermolecular self-assembly between the tectoRNA attenuator and the probe occurs when the PK-forming module interacts with the 3' side (in blue) of the receptor of the HD-forming module to form a 3' PK (equilibrium reaction between brackets). Interacting receptor (R) and loop (L) motifs as well as pseudoknot (PK) are indicated. (B) 3D stereo view scheme of the self-assembly equilibrium reaction for the tectoRNA 3'PK attenuator system. The formation of a PK between the PK-forming module and the 3' side of the receptor from the HD-forming module can prevent assembly of the HD-forming module with the GRAA probe.

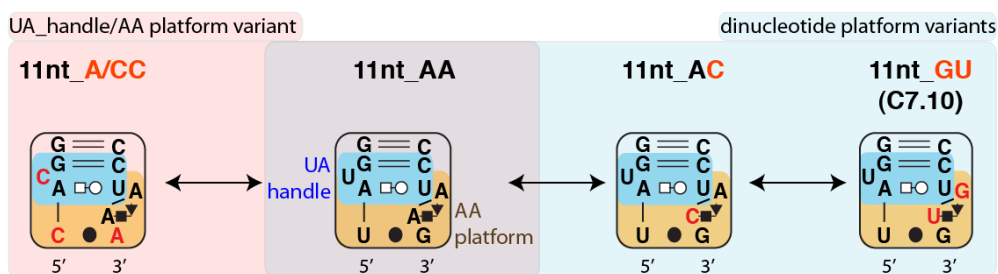


**Figure S2:** Structural modularity of the **11nt** receptor variants. These receptors are formed of two conserved G:C bps that form A minor interactions with the two last As from GAAA tetraloops (not shown) (15). The second module is a UA\_handle motif (in blue) that recognizes the second A from the GAAA (64). The U in bulge can theoretically be any nucleotide. The third module is a dinucleotide platform that stabilizes the second A of the GAAA through stacking interactions (21). While not as abundant than AA platforms, the AC and GU platform variants are both found in nature, with the AC platform being more abundant than the GU one in group I and group II introns (6,8). The G:U closing base pair can sometimes be substituted by the isosteric C:A(+) bp (6,8). Base-pairings are indicated according to Leontis and Westhof annotation (62).

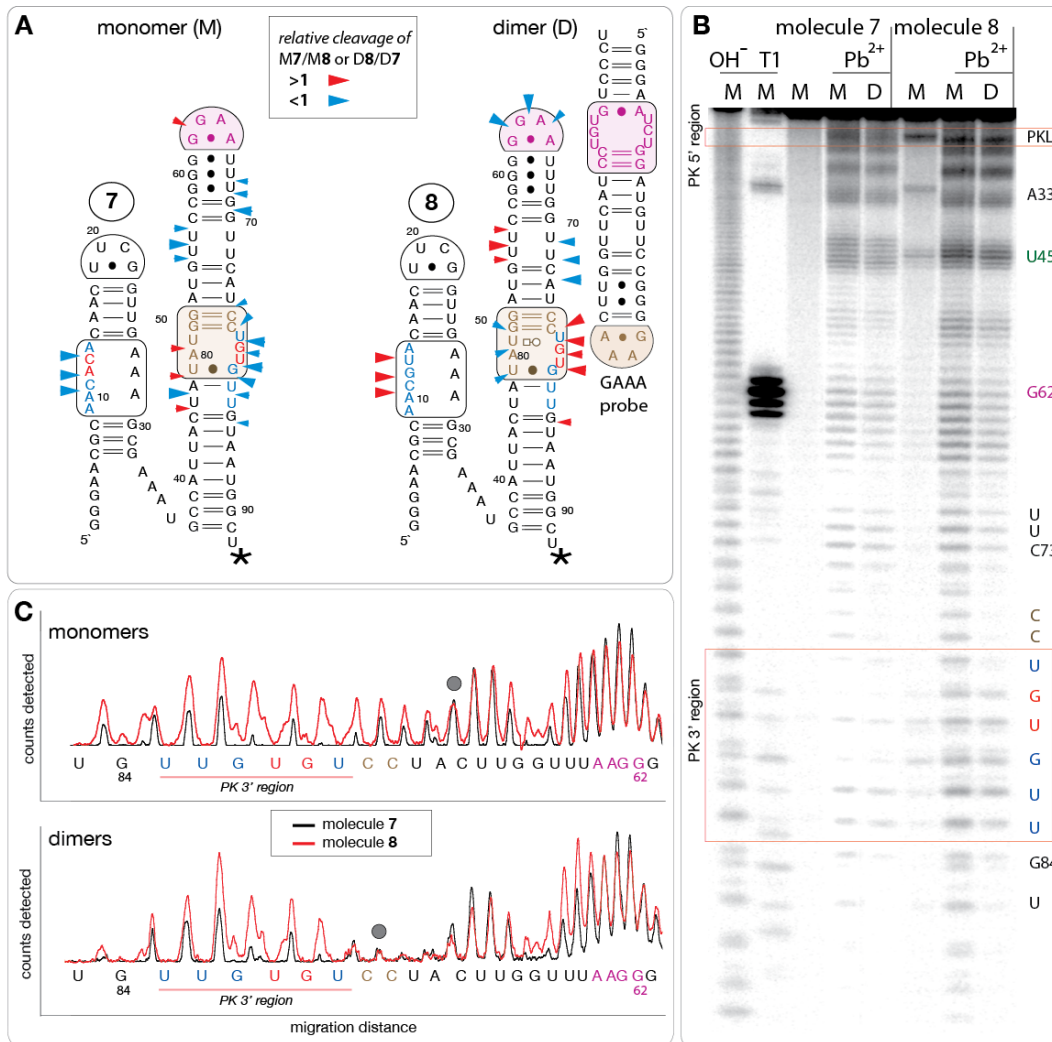


**Figure S3:** Lead(II)-induced cleavage patterns for tectoRNA attenuators **7** and **8** in their monomeric and heterodimeric states. **(A)** 2D diagrams of tectoRNA attenuators with reported differential Pb(II) cleavage patterns in the monomeric (M) and heterodimeric (D) states. Phosphate positions in monomer **7** (M7) that show enhanced or reduced Pb(II) cleavage with respect to monomer **8** (M8) are indicated by red or blue arrows on the 2D diagram of **7**, respectively. Phosphate positions in heterodimer **8** (D8) that show enhanced or reduced Pb(II) cleavage with respect to heterodimer **7** (D7) are indicated by red or blue arrows on the 2D diagram of **8**, respectively. The size of the arrows is roughly proportionate to the difference in cleavage for M7 versus M8 or D8 versus D7. A star indicates the radiolabeled RNA 3' end. **(B)** Pb(II) cleavage patterns of <sup>32</sup>P radiolabeled molecules **7** and **8** either alone or bound to their non-radioactive cognate GAAA probe (as shown in (A)). M and D correspond to monomer and dimer lanes, respectively. Cleavage experiments (indicated by Pb<sup>2+</sup>) were carried out as described in the Materials and Methods section; OH<sup>-</sup> indicates alkaline hydrolysis ladder; T1 indicates RNaseT1 digestion. **(C)** Superposed lead cleavage profiles for monomers **7** and **8** (top) and for the corresponding heterodimers in presence of GAAA probe (bottom). Black dots indicate positions used for normalization.



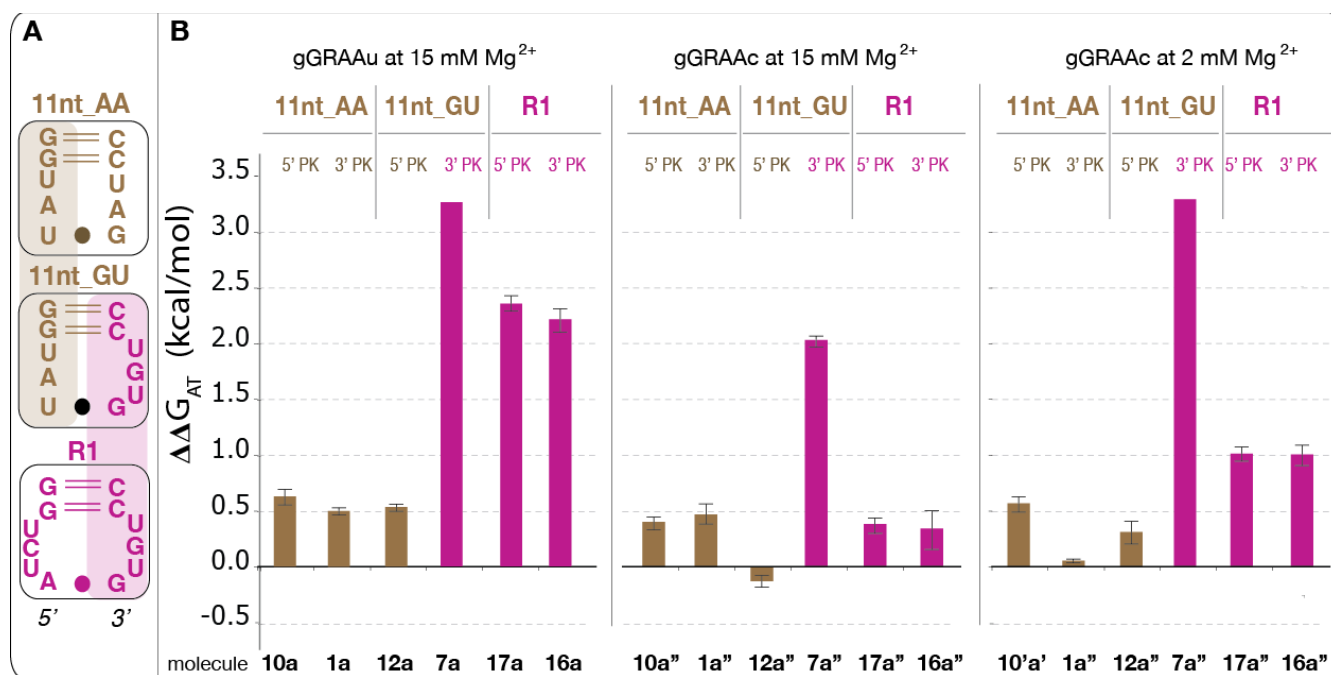


**Figure S4:** Thermodynamic analysis of tectoRNA attenuators based on the 11nt and R1 receptors. This tectoRNA series has PK internal loops (PKL) with five As instead three (see Table S1). **(A)** Sequence relationships between the R1 (15), 11nt\_GU (or C7.10 (8,15)) and 11nt receptors. **(B)** Free energies of attenuation of heterodimer formation for all attenuator constructs based on the 11nt and R1 receptors (see also Table S4). The free energies of attenuation ( $\Delta\Delta G_{AT}$ ) were estimated at 10°C and 2 or 15 mM Mg(OAc)<sub>2</sub> as described in Materials and Methods. Attenuators **1a''**, **7a''**, **10a''**, **12a''**, **16a''** and **17a''** differ from molecules **1a**, **7a**, **10a**, **12a**, **16a** and **17a** by the presence of gGRAAC terminal loops (instead gGRAAU). This single nucleotide variation increases heterodimer stability. No major differences are observed between these constructs, with PKL of 5 As, and those with PKL of 3 As (see Figure 5).

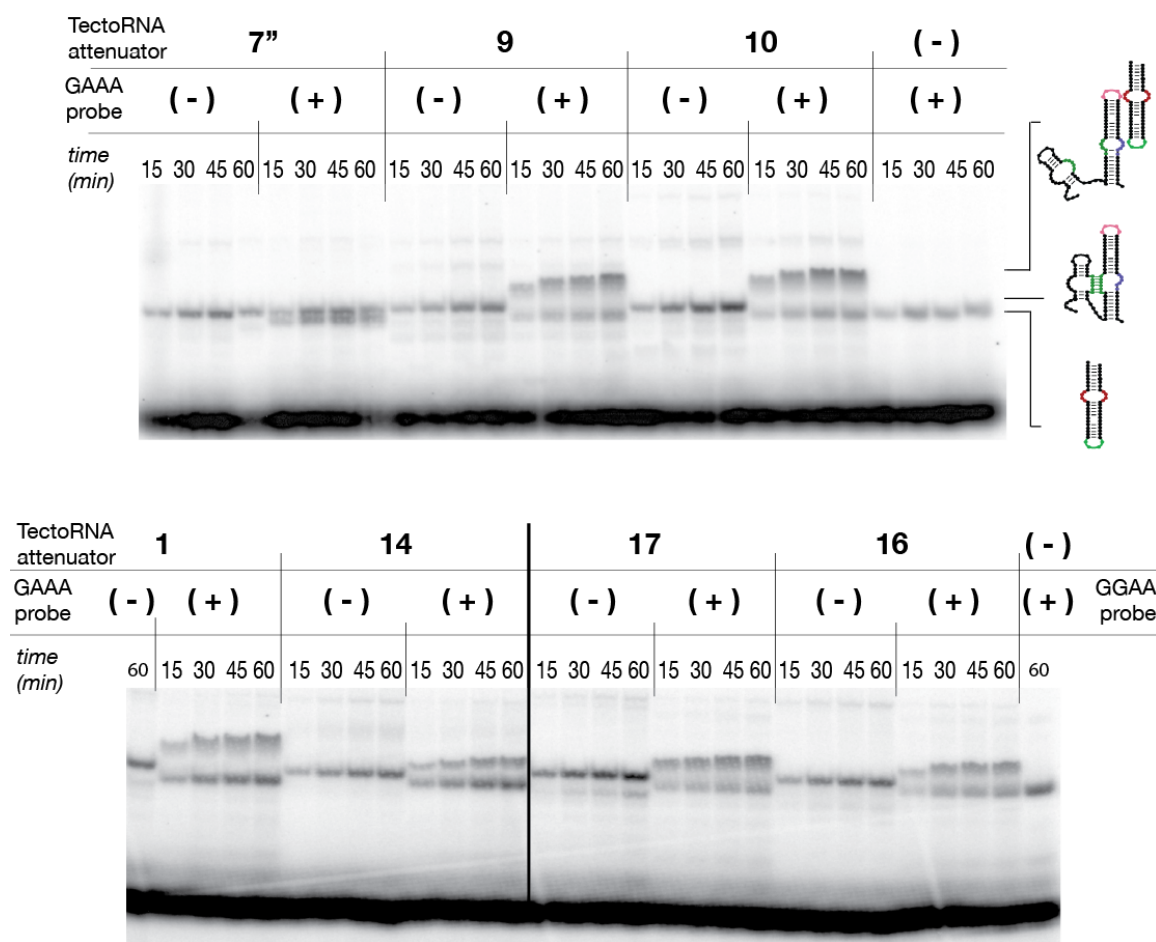


**Figure S5:** Co-transcriptional assemblies of tectoRNA attenuators **1**, **7''**, **9**, **10**, **14**, **16** and **17** in presence (or absence) of their cognate GAAA or GGAA probe. Native PAGE autoradiograms of different tectoRNA attenuator transcription mixtures at various times in presence (+) or absence (-) of probe are shown. Co-transcriptional assembly is monitored by RNA body-labeling with  $\alpha$ [P<sup>32</sup>]ATP and native PAGE is performed at 10°C and 10 mM Mg(OAc)<sub>2</sub> after quenching the transcription with DNase as described in Materials and Methods.

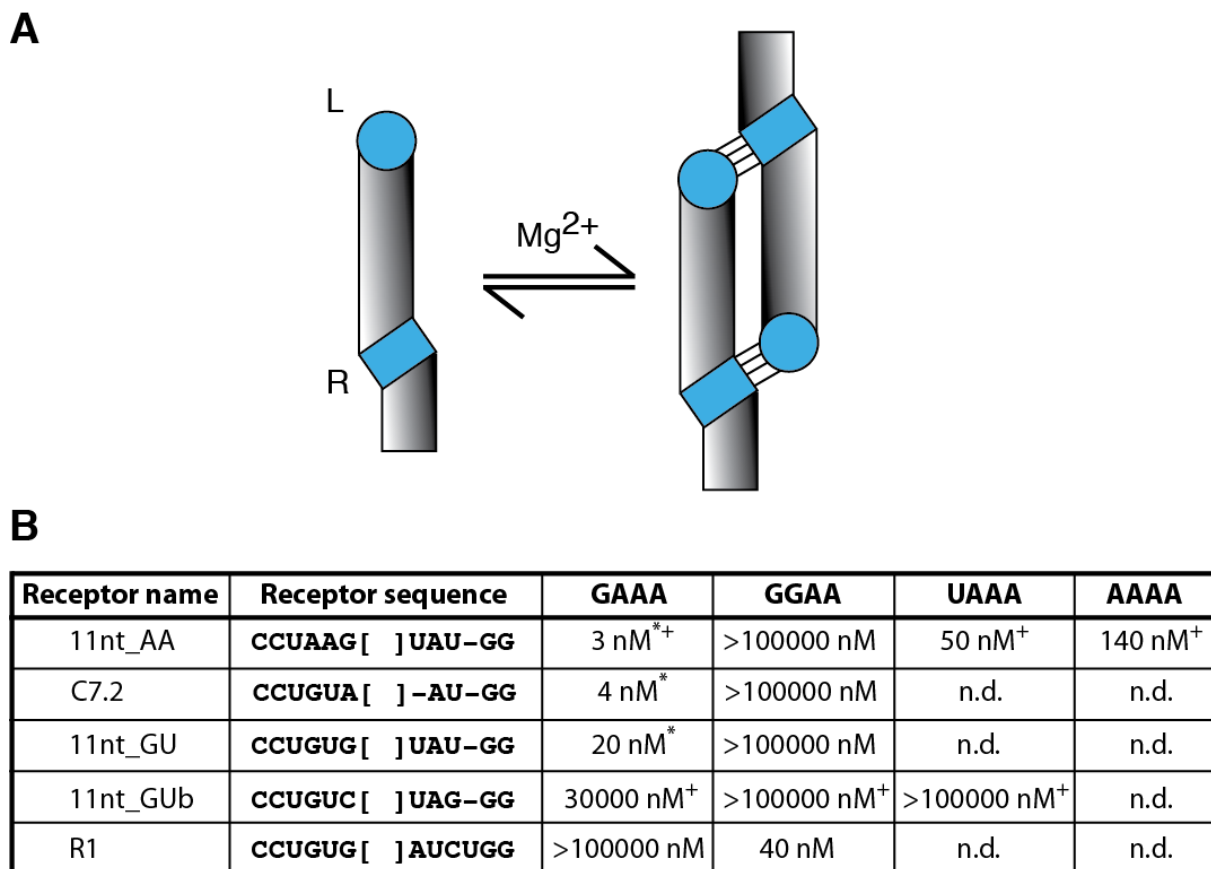


**Figure S6:** *In vitro* tectorNA self-assembly into homodimers. Most of these tectorNAs are based on receptors identified in class 1 di-GMP riboswitches (20). These results indicate that the GNRA/receptor interaction within this natural molecule can span a broad range of binding affinities. During evolution, it is unlikely that the bias towards “U/A-rich” receptors is therefore due to a selection pressure for an intrinsic stability or/and loop selectivity of the receptor. Indeed, this GNRA/receptor interaction is tunable so that the riboswitch can function in different gene regulatory contexts more as a dimmer or rheostat than a binary on of switch. **(A)** Self-assembly scheme. **(B)** Table with apparent equilibrium dissociation constants ( $K_d$  in nM) for various homodimer constructs of the type: R(receptor):(LGAAA), R(receptor):(LGGAA), R(receptor):(LUAAA), R(receptor):(LAAAA). \*: Indicates values previously reported in (15); +: Indicates that the loop/receptor combination is found in the context of the di-GMP riboswitch (20). The combination **GAAA** loop/ **11nt\_A/CC** is also found in the di-GMP riboswitch and has been characterized in the HD heterodimer context (Table S2). Note that for homodimers,  $K_d$ s were determined from a nonlinear fit of the experimental data to equation:  $f = (4\beta M_0 + K_d - (8M_0\beta K_d + K_d^2)^{0.5}) / 4M_0$ . With  $\beta$  typically equal to 1, the  $K_d$ 's equation is:  $K_d = ((2M_0)(1 - f)^2) / f$ . Therefore,  $K_d$ s correspond to  $M_0$  when 50% of bi-molecular assemblies are formed (15,23).

### C. Supplementary references

63. Bindewald, E., Kluth, T. and Shapiro, B.A. (2010) CyloFold: secondary structure prediction including pseudoknots. *Nucleic acids research*, **38**, W368-372.
64. Jaeger, L., Verzemnieks, E.J. and Geary, C. (2009) The UA\_handle: a versatile submotif in stable RNA architectures. *Nucleic Acids Res*, **37**, 215-230.